CAGEO : 994
pp.1–7 (col.fig.: NIL)
PROD.TYPE: COM
ED: SHANTA
PAGN: BMP SCAN: VINOD

PERGAMON

Computers & Geosciences 0 (2001) 1–7

COMPUTERS & GEOSCIENCES

Application and processing of geophysical images for mapping faults

Donat Demanet[a], Eric Pirard[b,*], François Renardy[a], Denis Jongmans[a]

[a] *Laboratories of Engineering Geology, Hydrogeology and Geophysical Prospecting, Liège University, Bât. B19, Sart-Tilman, B-4000 Liège, Belgium*

[b] *MICA, Geomaterials Characterisation Laboratory, Liège University, Bât. D2, Avenue des Tilleuls 45, B-4000 Liège, Belgium*

Received 14 September 1999; received in revised form 17 March 2000; accepted 21 March 2000

Abstract

This paper describes the application of geophysical prospecting techniques to locate the active faults in superficial quaternary sediments. Both electrical tomography and seismic refraction tomography presented here were part of a geophysical campaign performed in the Roer Graben area as a reconnaissance tool before trenching for paleoseismological observations. The aim of this investigation was, in the first place, to determine the exact position of the active fault in order to determine the best emplacement of a later trench. An additional objective was to image the fault zone at shallow depth, allowing both a comparison with trench data, and a downward extrapolation of these direct observations. Both methods proved to be successful but generated relatively smooth images with a poor spatial resolution that were prone to a subjective interpretation by the operators. In order to restrict the interpretation of tomographies with quantitative measures of gradients, image analysis techniques were tested. This paper presents some preliminary results obtained on the use of crest line location methods issued from mathematical morphology. Synthetic models of simple resistivity anomalies along a faulted section were used to check the reliability of the image processing method.

Keywords: Electrical tomography; Seismic refraction tomography; Gradient; Watershed divide line

1. Introduction

Even when a geomorphological expression of a fault is present in the topography, the fault trace is often difficult to locate accurately. Non-destructive geophysical prospecting techniques may then be applied in order to map the fault trace with accuracy in the superficial sediments. During the last few years, a large number of high-resolution seismic reflection surveys have been conducted (see e.g., Williams et al., 1995; Palmer et al., 1997; Van Arsdale et al., 1998) to provide information on quaternary fault geometry and timing in different areas. For a very shallow investigation, ground-penetrating radar (GPR) has been recently applied by Cai et al. (1996) in the San Francisco Bay region. At the border of Nevada and California, Shields et al. (1998) employed several geophysical techniques (seismic reflection, magnetics and electromagnetics) to locate the extension of the Parhump Valley fault zone. All these applications rely on visual interpretation for location of fault traces and this underlines the fact that although image analysis is now commonplace in many geological imaging applications, a lot of research work still has to be performed to take advantage of quantitative methods in geophysical image analysis. A recent presentation by Liner (1999) promoted the use of imaging freewares for implementing simple geophysical image processing tools. In addition to directional shadow processing and

*Corresponding author. Tel.: +32-4-366-9528; fax: +32-4-366-9520.

E-mail addresses: ddemanet@ulg.ac.be (D. Demanet), eric.pirard@ulg.ac.be (E. Pirard), djongmans@ulg.ac.be (D. Jongmans).

0098-3004/01/$ - see front matter
PII: S0098-3004(00)00156-4

pseudo-colour enhancement, the major interest of imaging softwares is to be developed in the segmentation tools available for identification and localization of anomalies. A preliminary exploration of the potential of both gradients and watersheds in geophysical images is illustrated hereafter.

2. Electrical tomography

Electrical tomography is a 2D imaging technique showing the variations in the ground resistivity along a section. It is based on the same principles as such other classical electrical methods like sounding or profiling. A controlled current (I) is injected into the ground with two electrodes, while measuring the potential (V) between two other electrodes. The resistance is calculated using Ohm's law. The material parameter resistivity (ρ), which is the inverse of electrical conductivity (σ) is related to the resistance via a geometrical factor. To build an electrical image of the ground (a 2D section of resistivity), numerous measurements are carried out for various combinations of potential and current electrodes. The Wenner configuration (constant offset between electrodes) has been used. The first step in the data interpretation consists in building a pseudo-section obtained by plotting the apparent resistivity versus the depth (proportional to the offset between electrodes) for each midpoint of a given electrode configuration. This representation leads to a qualitative image where neither the resistivities nor the depths are correct.

It is necessary to inverse the pseudo-section in order to determine a vertical resistivity section as a function of a true depth. The inversion of the data is carried out according to an iterative process which aims at minimising the difference between the measured pseudo-section and a calculated pseudo-section based on a model. This model is updated after each iteration until reaching an acceptable agreement between measured and calculated data or until no further improvement is possible. The data are processed with the algorithm proposed by Loke and Barker (1996) implemented in the RES2DINV software. Fig. 1 shows the results of a survey performed at Jülich (Germany) across the escarpment of the Peel fault. The aim of this investigation is to determine the exact position of the fault as well as to image the fault zone at shallow depth. This work has been realised in collaboration with the Geological Survey of North-Westphalia and the University of Köln. The field measurements were performed with ABEM devices: Electrode Selector ES-464 and Terrameter 300C. Four cables with an amount of 64 connectors were extended along the profile. With a 2 m constant electrode offset, this provides a total length of 126 m. Fig. 1 very clearly highlights a sharp lateral variation of resistivity at about 60 m. The top of the escarpment is more resistive than the bottom.

3. Seismic refraction tomography

The test site was selected based on a preliminary paleoseismological study in the Roer Graben near the city of Bree (NE of Belgium). In the framework of this project, several geophysical measurements were carried out across the escarpment of a presumed active fault in order to locate and to image the fault zone. The results combined with the dig of an 80 m long and 3.5 m deep trench revealed two faults separated by 25 m (Demanet et al., 2000).

The first step in the refraction tomography survey consists of measuring first-arrival times between sources and receivers located along a profile crossing the fault escarpment. Combining travel-times from a number of sources and receivers at different positions along the profile, one can determine the P-wave velocity

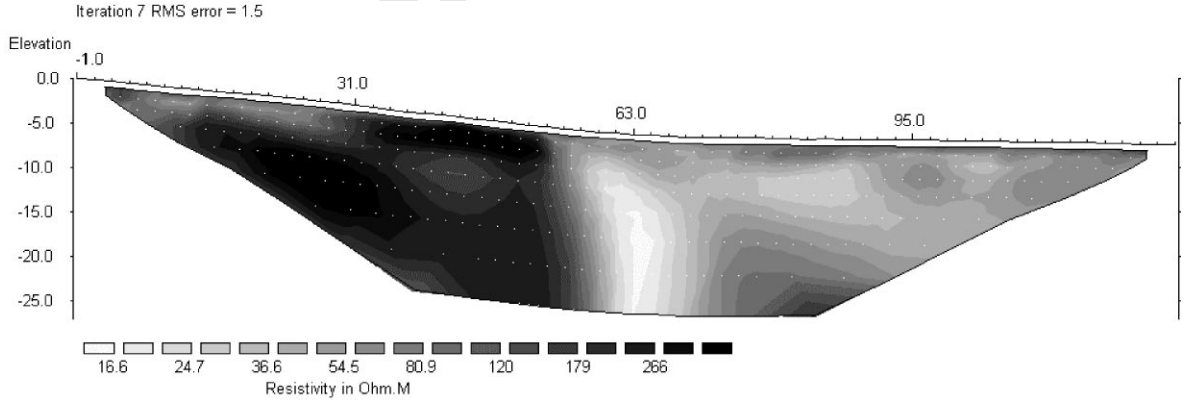

Fig. 1. Electrical tomography (after inversion) across escarpment of presumed active fault in Jülich. Subjective choice of colour palette has important impact on visual localisation of anomalies.

distribution on a two-dimensional section. Various numerical inversion schemes have been proposed for image reconstruction (see Ivansson, 1987). In this study, we have used the simultaneous iterative reconstruction technique (SIRT) developed by Gilbert (1972). In this iterative method, which is presented in detail by Krajewski et al. (1989), a first guess of the solution is assumed and the theoretical travel-times are computed for each ray. The residuals between calculated and observed times are then used to correct the velocity values along the ray path, giving a new image. The iterative procedure is stopped when some criteria are met; for instance when the rms (root mean square) of the residual travel-times is assessed as low enough. Our software, developed in-house, uses curved rays computed from the gradient of the travel time on the whole grid. The acquisition configuration was 96 m long with one receiver every 2 m. The source was a hammer with a shot-point at each geophone position. Data were stacked at least six times for each source. The starting model of the inversion process was based on the results of a classical seismic refraction profile along the fault escarpment. The inversion process was stopped after 10 iterations. The stopping criteria were the rms and the standard error of both the residual travel-times and the velocity variations between two iterations. Results of the inversion are presented in Fig. 2. Two sharp dipping anomalies are situated around 70 and 95 m, exhibiting a stair-shaped section and correlating very well with the preliminary geophysical study and the trench observations.

4. Image processing

4.1. From geophysical data to raster image files

In order to fit with the requirements of most image processing algorithms, geophysical data had to be converted into 256 grey levels (8 bits) bitmap format. This led to an obvious loss of resolution in the grey level dynamic, but it was considered, in a first approach, as an acceptable approximation. Original resistivity values were in the range between 0 and 300 Ω m but with two significant digits that would require 16 bits of depth to be taken into account. The spatial resolution of the images was controlled by the grid of the inversion process, being typically 60×20 pixels for electrical tomographies and 48×20 for seismic refraction tomographies. The systematic gridding of the inversion process does not take into account the limits imposed by topography as well as the decrease in lateral extent towards greater depth. This means that all data in the rectangular raster image files (Fig. 3) are not relevant and will have to be masked at the end of the image processing procedure by a field of validity (see the trapezoidal shape in Fig. 1). Geophysical data imported as raster files (*.bmp) were processed and analysed with routines developed within Micromorph (Beucher, 1995).

4.2. Goals of the image processing strategy

At first glance, the geophysical images display variable intensities reflecting various lithologies. When searching for fault zones, it is not that much the absolute intensities that are to be determined but merely the abrupt transitions between lithological units that have

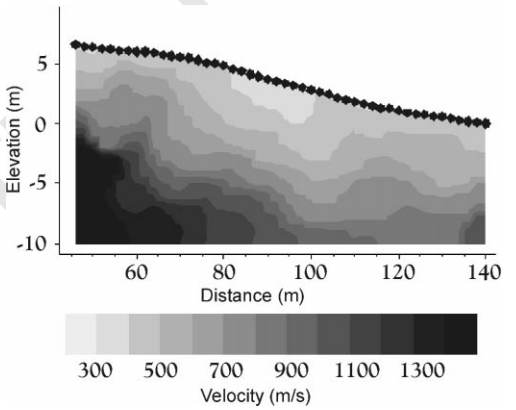

Fig. 2. Seismic refraction tomography image from Bree fault escarpment.

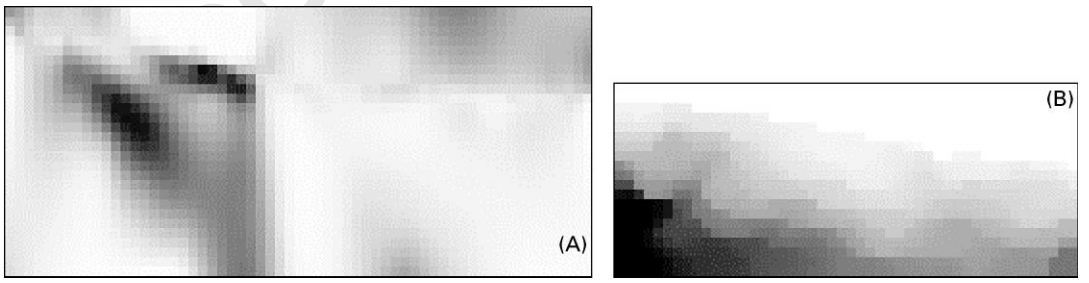

Fig. 3. Original image files used as input of image processing routines. (A) Jülich electrical tomography ($61 \times 28 \times 8$ bits) and (B) Bree seismic refraction tomography ($48 \times 20 \times 8$ bits).

to be identified. Therefore, the philosophy behind the image processing strategy can be translated in terms of

(1) filtering of raw data,
(2) gradient computation,
(3) location of crest lines within the gradient image.

The final result will be a binary image wherein the position of pixels will delimit the probable existence of a fault. Working with poor resolutions and without sub-pixel accuracy algorithms (Van Vliet, 1993), one must accept the result as being a jagged line giving a rough guess of the fault location. In order to somehow check the relative accuracy of various image processing alternatives, synthetic images were built from simple models of resistivity (Fig. 4).

4.3. Gradient computations

Any kind of gradient computation is strongly affected by noise and it is common practice to first perform a spatial filtering operation. In the present case, however, the geophysical data have been subject to interpolation during their inversion. This precludes the need for any further low-pass smoothing in the image processing context, but points out that the original filtering, beyond the control of the authors in the case of electrical tomographies, might have a strong influence on the final results and should be considered as an important parameter for judging the adequacy of the image processing procedure in the future.

Gradient images can be computed using several approaches starting from the most popular Sobel and Prewitt convolution kernels (Russ, 1999) to the most sophisticated Canny-Deriche filters (Canny, 1986). Facing the problem of very poor spatial resolutions and having no "a priori" on the shape of transitions between high and low resistivity units, it was decided to first explore images with morphological gradients. A morphological gradient as defined by Beucher and Meyer (1992) is the arithmetical difference between dilation (maximum grey level) and erosion (minimum grey level) within a given structuring element. In the vocabulary of mathematical morphology, a structuring element can be any kind of user-defined local geometry. In practice, this definition gives rise to either directional or non-directional gradients of various sizes (Fig. 5).

The reason for working with morphological gradients is that they are being easily computed and that they take advantage of the theoretical background of mathematical morphology. However, when increasing the size of the neighbourhood, the problem of delocalisation of the grey-level transition and of non-normalisation with respect to the distance between pixels may become prohibitive. The idea of working with a supremum of directional gradients forced to pass through the central pixel and normalised with respect to the real distance between minimum and maximum grey levels has been further explored using 32 bit images but due to the need of developing floating point watershed algorithms, the real benefit of working with such gradients could not be assessed at this point. Fig. 6 displays a comparative view of several morphological gradients computed on the electrical tomography of Fig. 3A. Broadening the width of the gradient from 3×3 to 5×5 is clearly helpful for a better localisation of the crest lines, but due to non-normalisation of the gradients this must be handled carefully. Wider gradients are not realistic due to the poor resolution of the original geophysical data. Fig. 6D

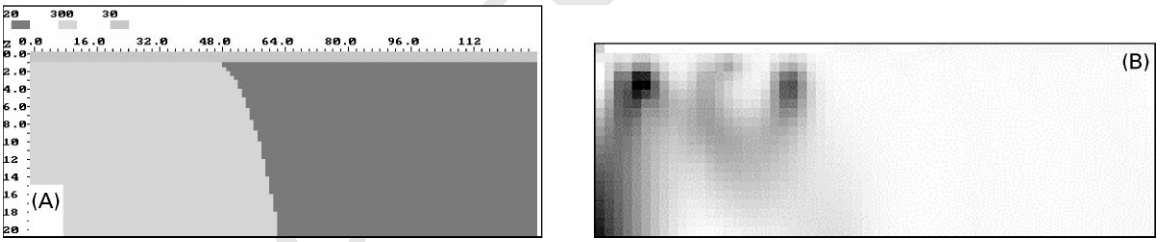

Fig. 4. Simple model with oblique fault separating domains of 300 and 20 Ω m overlaid by 30 Ω m layer (A) and corresponding synthetic resistivity image obtained after inversion (B).

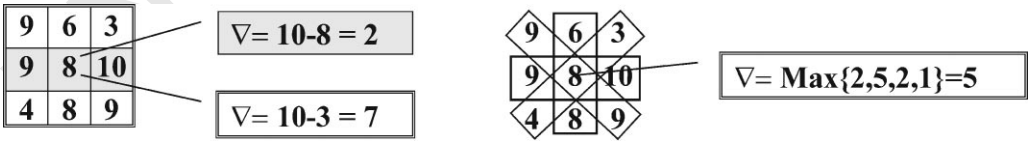

Fig. 5. Morphological gradient on 3×3 neighbourhood replaces central pixel by difference between its greatest and smallest neighbours ($\nabla = 7$). Horizontal gradient of size 1 (greyish neighbourhood) gives $\nabla = 2$, whereas supremum of directional gradients of size 1 takes value $\nabla = 5$. Notice that none of these gradients really pass through central pixel of neighbourhood.

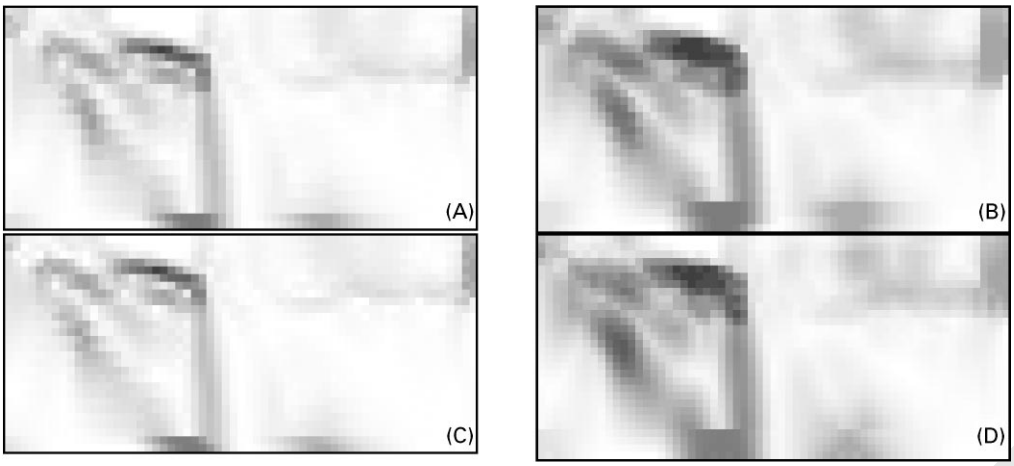

Fig. 6. Several gradients from electrical tomography taken in Jülich (Fig. 1): (A) morphological gradient on 3×3 neighbourhood; (B) id. on 5×5 neighbourhood; (C) supremum of directional gradients of size 1; (D) supremum of directional gradients of size 2 forced to pass through central pixel.

is a supremum of directional gradients of size 2 (5 pixels width) wherein minimum and maximum were forced to be on both sides of the central pixel.

4.4. Crest lines identification

Considering the gradient images as a topographical relief, one can express the interesting features as being crest lines. This is a very common problem in any kind of imaging that has been addressed in several ways among which grey-level skeletonisation, hierarchical tophats, snakes or watershed divide lines. Most often, these techniques result in an oversegmentation of the image and the main problem is to remove significant crest lines without altering noisy crest lines.

The watershed divide line, as defined by Beucher and Meyer (1992), was chosen here because of its flexibility particularly in its marker-based approach. Basically it consists in building a dam on the grey-level image, considered as a relief, in order to avoid mixing of fluids flowing from different sources. These sources can be either true local minima in the image or any kind of user defined marker (see applications of the swamping technique in Serra, 1995).

In the present case, the markers to be used as input for the location of faults within the gradient image are the "geological units". These should correspond to homogeneous responses in resistivity or in other words, to very low values of the gradient. Therefore, the markers of the different geological units are extracted using a simple thresholding of the gradient image. A typical threshold for eliminating too large gradients was set at values close to 5–15 gradient units (less than 6% of the 8-bits dynamic).

As seen from Fig. 7, it occurs quite often that markers are found very close to each other and that they cannot be clustered together without increasing the threshold, thereby deteriorating the whole image. Considering from the principle of the watershed that any two sources will be separated by a crest line, it is important to find a local criterion for clustering markers together. This is performed by adding a marker growing step to the thresholding operation. As illustrated in Fig. 8, the

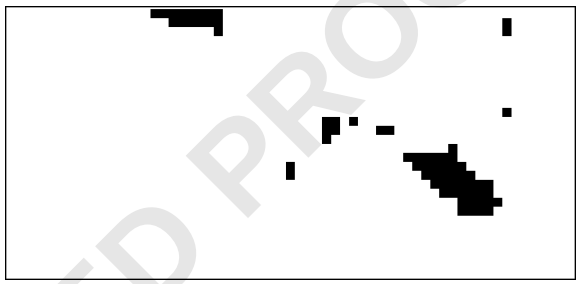

Fig. 7. Extraction of very low-gradient units by thresholding Fig. 6D at level 7.

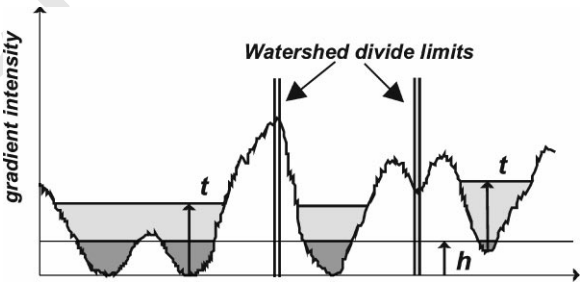

Fig. 8. Section in gradient image illustrating principles of minimum gradient detection. After propagation within tolerance of t grey levels, initial four markers obtained from thresholding at level h are left as three significant markers thus reducing number of necessary watershed divide lines.

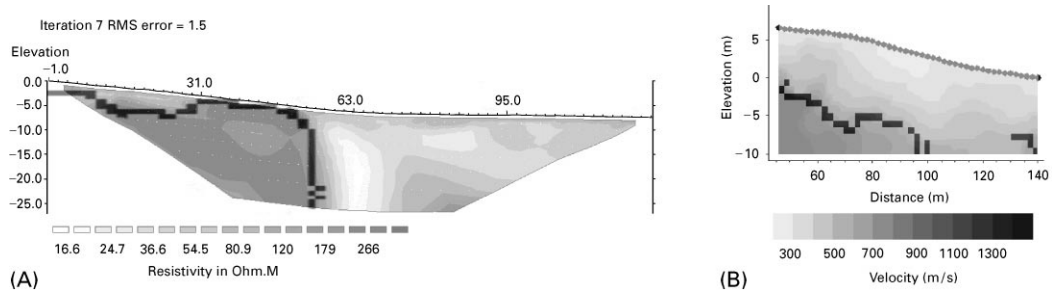

Fig. 9. Conditional watershed delineation (dark line) of strong discontinuities in Jülich resistivity image (A) and Bree fault escarpment seismic refraction image (B).

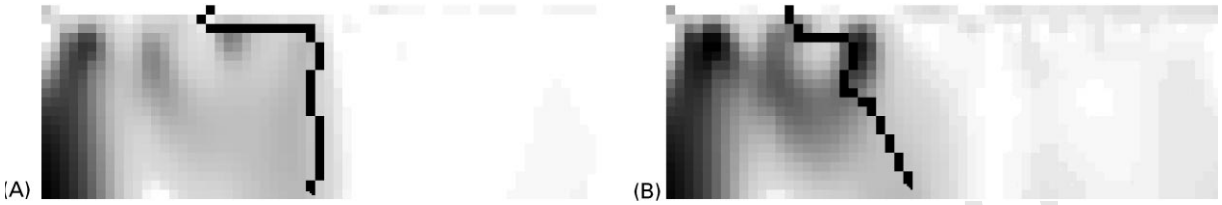

Fig. 10. Conditional watershed delineation (dark line) within synthetic resistivity images. Vertical fault model (A) and oblique fault model from Fig. 4B (B).

original markers obtained from thresholding at value h, are allowed to propagate as long as they stay within a given gradient intensity tolerance (typically 10–20 units). The final result is such that low gradient markers that were only separated by a crest below the tolerance limit were allowed to cluster together into a unique marker. The extended-minima-controlled watershed segmentation has been tested on both, the electrical tomography and the seismic tomography, and the synthetic cases (Figs. 9 and 10).

5. Conclusions

The image processing methodology proposed in this paper clearly demonstrates its capacity to identify faults within both kinds of geophysical images. The process is still user-dependent in the sense that both threshold values and tolerance values will have an impact on the final result. When contrast is diminishing, the result may become unstable with respect to the operators choice.

Further work is needed to explore more accurate gradient computations such as multiscale and normalised gradients. Existing algorithms have to be improved for dealing with floating point images and for allowing sub-pixel accuracy in the watershed divide line location. The watershed algorithm itself should be improved by using a parallel computation technique avoiding misplacement of the divide line (Beucher, pers. comm.). Finally, a hierarchy of divide lines based on their gradient intensities should be delivered as an output instead of a binary fault/non-fault response.

6. Uncited Reference

Docherty 1992.

Acknowledgements

Part of this project was realised under the contract ENV4-CT97-0578 funded by the European Commission. We also wish to thank the Royal Observatory of Belgium for its contribution.

References

Beucher, S., 1995. Micromorph, un logiciel d'apprentissage de la Morphologie Mathématique. In: Images Numériques dans l'Enseignement des Sciences. Journées d'études INRP/CNAM, pp. 77–80.

Beucher, S., Meyer, F., 1992. The morphological approach to segmentation: the watershed transformation. In: Dougherty, E. (Ed.), Mathematical Morphology in Image Processing. Marcel Dekker, New York, pp. 433–481.

Cai, J., McMechan, A., Fisher, M.A., 1996. Application of ground penetrating radar to investigation of near-surface fault properties in the San Francisco bay region. Bulletin of the Seismological Society of America 86, 1459–1470.

Canny, J., 1986. A computational approach to edge detection. IEEE Transactions on Pattern Analysis and Machine Intelligence 8 (6), 679–698.

Demanet, D., Renardy, F., Vanneste, K., Jongmans, D., Camelbeeck, T., Meghraoui, M., 2000. The use of geophysical prospecting for imaging active faults in the Roer Graben, Belgium. Geophysics, for publication.

Docherty, P., 1992. Solving for the thickness and velocity of the weathering layer using 2D refraction tomography. Geophysics 57, 1307–1318.

Gilbert, P., 1972. Iterative methods for the three-dimensional reconstruction of an object from projections. Journal of Theoretical Biology 36, 105–117.

Ivansson, S., 1987. Cross-hole transmission tomography. In: Nolet, G. (Ed.), Seismic Tomography. D. Reidel Publishing Company, Dordrecht, pp. 159–188.

Krajewski, C., Dresen, L., Gelbke, C., Ruter, H., 1989. Iterative tomographic methods to locate low-velocity anomalies: a model study. Geophysical Prospecting 37, 717–751.

Liner, C., 1999. Geophysics and NIH image. Computers & Geosciences 25, 403–414.

Loke, M.H., Barker, R.D., 1996. Rapid least-squares inversion of apparent resistivity pseudo-sections by quasi-Newton method. Geophysical Prospecting 44, 131–152.

Palmer, J.R., Shoemaker, M., Hoffman, D., Anderson, N.L., Vaughn, J.D., Harrison, R.W., 1997. Seismic evidence of quaternary faulting in the Benton hills area, southeast Missouri. Seismological Research Letters 68, 650–661.

Russ, J.C., 1999. The Image Processing Handbook, 3rd Edition. CRC-Springer-IEEE Press.

Serra, J., 1995. Morphological image segmentation. Acta Stereologica 14/2, 99–111.

Shields, G., Allander, K., Brigham, R., Crosbie, R., Trimble, L., Sleeman, M., Tucker, R., Zhan, H., Louie, J.N., 1998. Shallow geophysical survey across the Pahrump Valley fault zone, California–Nevada border. Bulletin of the Seismological Society of America 88, 270–275.

Van Ardsale, R., Purser, J., Stephenson, W., Odum, J., 1998. Faulting along the southern margin of Reeflot lake, Tennessee. Bulletin of the Seismological Society of America 88, 131–139.

Van Vliet, L., 1993. Grey scale measurements in multi-dimensional digitized images. Ph.D. Dissertation, Delft University Press.

Williams, R.A., Luzietti, E.A., Carver, D.L., 1995. High-resolution imaging of Quaternary faulting on the Crittenden County fault zone, New Madrid seismic zone, northeastern Arkansas. Seismological Research Letters 66, 42–57.